

Opacity Broadening of ^{13}CO Linewidths and its Effect on the Variance-Sonic Mach Number Relation

C. Correia¹, B. Burkhart², A. Lazarian², V. Ossenkopf³, J. Stutzki³, J. Kainulainen⁴, G. Kowal⁵ and J. R. de Medeiros¹

¹ *Departamento de Física Teórica e Experimental, Universidade Federal do Rio Grande do Norte, 59072-970, Brazil; e-mail: caioftc@dfte.ufrn.br*

² *Astronomy Department, University of Wisconsin, Madison, 475 N. Charter St., WI 53711, USA*

³ *Physikalisches Institut der Universität zu Köln, Zùlpicher Strasse 77, 50937 Köln, Germany*

⁴ *Max-Planck-Institute for Astronomy, Königstuhl 17, 69117, Heidelberg, Germany*

⁵ *Instituto de Astronomia, Geofísica e Ciências Atmosféricas, Universidade de São Paulo, 05508-090, Brazil*

ABSTRACT

We study how the estimation of the sonic Mach number (M_s) from ^{13}CO linewidths relates to the actual 3D sonic Mach number. For this purpose we analyze MHD simulations which include post-processing to take radiative transfer effects into account. As expected, we find very good agreement between the linewidth estimated sonic Mach number and the actual sonic Mach number of the simulations for optically thin tracers. However, we find that opacity broadening causes M_s to be overestimated by a factor of $\approx 1.16 - 1.3$ when calculated from optically thick ^{13}CO lines. We also find that there is a dependency on the magnetic field: super-Alfvénic turbulence shows increased line broadening as compared with sub-Alfvénic turbulence for all values of optical depth for supersonic turbulence. Our results have implications for the observationally derived sonic Mach number–density standard deviation ($\sigma_{\rho/\langle\rho\rangle}$) relationship, $\sigma_{\rho/\langle\rho\rangle}^2 = b^2 M_s^2$, and the related column density standard deviation ($\sigma_{N/\langle N \rangle}$) sonic Mach number relationship. In particular, we find that the parameter b , as an indicator of solenoidal vs. compressive driving, will be underestimated as a result of opacity broadening. We compare the $\sigma_{N/\langle N \rangle}$ – M_s relation derived from synthetic dust extinction maps and ^{13}CO linewidths with recent observational studies and find that solenoidally driven MHD turbulence simulations have values of $\sigma_{N/\langle N \rangle}$ which are lower than real molecular clouds. This may be due to the influence of self-gravity which should be included in simulations of molecular cloud dynamics.

Subject headings: ISM: structure — magnetohydrodynamics (MHD) — methods: numerical

1. Introduction

Supersonic magnetized turbulence is observed in multiple tracers across several different interstellar media (ISM) phases. This includes the neutral medium, as traced by HI (see Chepurnov et al. 2010; Burkhart et al. 2010; Peek et al. 2011), the warm ionized medium, as traced by H α (see Hill et al. 2008), electron density fluctuations (Armstrong et al. 1995; Chepurnov & Lazarian 2010), synchrotron polarization (Gaensler et al.

2011; Burkhart et al. 2012) and the molecular medium (see Heyer et al. 1998; Goldsmith et al. 2008), which includes a variety of molecular traces including the often used carbon monoxide (CO) line.

Turbulence and magnetic fields in these environments are interrelated to a variety of physical process, including cosmic ray transport (Yan & Lazarian 2004; Beresnyak et al. 2011), magnetic reconnection (Lazarian & Vishniac 1999; Kowal et al.

2009), and star formation (McKee & Ostriker 2007, and ref. therein). Furthermore it is clear that, in order to understand MHD turbulence and related physical mechanisms, one needs to be able to measure basic plasma parameters such as the sonic and Alfvénic Mach numbers ($M_s \equiv V_{turb}/c_s$, where c_s is the sound speed, and $M_A \equiv V_{turb}/V_{Alfven}$, respectively).

It is clear from simulations, observations, and theoretical works that compressible turbulence, which generates shocks, is important for creating filaments and local regions of high density contrast (Kowal & Lazarian 2007). Shocks broaden the gas/dust density and column density probability distribution function (PDF) as well as increase the peaks and drag out the distribution’s tails towards higher gas densities (Burkhart et al. 2009). Based on this observation, several authors (e.g. Vazquez-Semadeni 1994; Padoan et al. 1997; Federrath et al. 2010; Burkhart & Lazarian 2012, to name a few) have developed relationships between the PDF moments, such as the variance or standard deviation of density ($\sigma_{\rho/\langle\rho\rangle}$), and the sonic Mach number, for example

$$\sigma_{\rho/\langle\rho\rangle}^2 = b^2 M_s^2 \quad (1)$$

where b is a parameter that depends on the type of turbulence forcing with $b=1/3$ for pure solenoid forcing and $b=1$ for pure compressive forcing (Federrath et al. 2008). Once gas becomes dense enough, collapse can occur via self-gravity and the PDF forms power-law tails towards higher density regions (Klessen et al. 2000; Collins et al. 2012). Additional variants of Equation 1 have also be developed, e.g. including plasma β (see Molina et al. 2012).

Eq. 1 is hard to constrain observationally as volume densities and the 3D velocity structure are not available from observations. Important information on turbulent supersonic motions in molecular clouds comes from the observed non-thermal broadening of the linewidths of different spectral lines, e.g. from carbon monoxide (CO) emission. However, CO, in particular ^{13}CO is often partially or fully optically thick and traces only a limited dynamic range of column densities (see Goodman et al. 2009; Burkhart et al. 2013b, b).

Fortunately, dust extinction column density maps of infrared dark clouds (IRDCs), includ-

ing mid infrared (MIR) and near infrared (NIR) wavelengths can be used to trace a much larger dynamic range of densities in order to probe the PDF ($A_v=1-25$ for NIR and $A_v=10-100$ for MIR, see Lombardi & Alves 2001; Kainulainen et al. 2011; Kainulainen & Tan 2013, henceforth KT13). However, extinction maps carry no dynamical information regarding velocities and for this, molecular line profiles are needed to measure the dynamics of clouds, including the sonic Mach number for a given cloud temperature.

In this paper we investigate the robustness of measuring the sonic Mach number from maps of ^{13}CO using synthetic observations derived from 3D MHD turbulence simulations. We further create synthetic dust maps in order to compare the PDF standard deviation with the measured sonic Mach number, following the approach in the observational work of KT13.

2. Numerical Data

We generate a database of twelve 3D numerical simulations of isothermal compressible (MHD) turbulence with resolution 512^3 (All models are listed in Table 1). For models with $M_s < 20$ we use the MHD code detailed in Cho & Lazarian (2003) with large scale solenoidally driven turbulence. Our two models with $M_s > 20$ are from the AMUN code (Kowal et al. 2011). The magnetic field consists of the uniform background field and a time-dependent fluctuating field: $\mathbf{B} = \mathbf{B}_{ext} + \mathbf{b}(\mathbf{t})$; $\mathbf{b}(\mathbf{0}) = \mathbf{0}$. For more details on the simulations scheme see Burkhart & Lazarian (2012, henceforth BL12) and Burkhart et al. (2013b).

Our models are divided in two groups corresponding to sub-Alfvénic ($B_{ext} = 1.0$) and super-Alfvénic ($B_{ext} = 0.1$) turbulence. For each group we compute five models with different gas pressures falling into subsonic and supersonic regimes with M_s ranging from 0.7 to 26 (see Table 1).

We post-process the simulations to include radiative transfer effects from the $^{13}\text{CO } J = 2 - 1$ line. For more information on this code and the assumptions involved see Ossenkopf (2002) and Burkhart et al. (2013b, b). Our original simulation set the sonic Mach number using the sound speed. We rescale our simulation’s velocity field in such a way that each have the same value of temperature and retain the original sonic

TABLE 1

DESCRIPTION OF THE 12 SIMULATIONS EACH WITH FOUR DIFFERENT DENSITY VALUES (GIVEN IN COLUMN ONE) IN ORDER TO PROBE VARYING OPTICAL DEPTH. COLUMNS TWO-FOUR GIVE CLOUD PARAMETERS FOR SUPER-ALFVÉNIC SIMULATIONS WHILE COLUMNS FIVE-SEVEN GIVE PARAMETERS FOR SUB-ALFVÉNIC SIMULATIONS. THOSE PARAMETERS ARE: THE 1D VELOCITY DISPERSION, ESTIMATED SONIC MACH NUMBER (SEE SECT. 2) AND THE AVERAGE OPTICAL DEPTH OF THE CLOUD GIVEN BY SIMLINE3D (SEE OSSENKOPF 2002). THE ACTUAL M_s AS MEASURED FROM THE ORIGINAL MHD SIMULATIONS WITH NO RADIATIVE TRANSFER IS SHOWN ABOVE EACH GROUP OF DENSITY SCALING FACTORS.

density	Super-Alfvénic ($M_A^a \simeq 7.0$)			Sub-Alfvénic ($M_A^a \simeq 0.7$)		
	σ_{13CO}^{1D} [kms $^{-1}$]	M_S^b	τ	σ_{13CO}^{1D} [kms $^{-1}$]	M_S^b	τ
	$M_S^c \simeq 26.2$			$M_S^c \simeq 25.3$		
9n	6.75	34.4	0.0017	4.21	21.5	0.0022
275n	6.29	32.1	0.03	3.85	19.6	0.092
8250n	6.25	31.9	1.2	4.77	24.4	2.5
82500n	6.42	32.8	2.0	5.64	28.8	29.6
	$M_S^c \simeq 9.0$			$M_S^c \simeq 7.9$		
9n	1.83	9.3	0.0066	1.26	6.4	0.0003
275n	1.92	9.8	0.3	1.41	7.2	0.3
8250n	2.20	11.2	3.0	1.76	9.0	3.2
82500n	2.32	11.8	54.7	1.94	9.9	74.4
	$M_S^c \simeq 7.1$			$M_S^c \simeq 6.8$		
9n	1.34	6.8	0.008	1.00	5.1	0.0037
275n	1.47	7.5	0.1	1.12	5.7	0.4
8250n	1.71	8.7	3.0	1.54	7.9	10.0
82500n	1.81	9.2	68.9	1.68	8.6	96.1
	$M_S^c \simeq 4.3$			$M_S^c \simeq 4.5$		
9n	0.84	4.3	0.0067	0.68	3.5	0.015
275n	0.84	4.3	0.3	0.85	4.4	0.4
8250n	1.00	5.1	13.0	1.09	5.6	13.0
82500n	1.06	5.4	56.6	1.18	6.0	128.0
	$M_S^c \simeq 3.1$			$M_S^c \simeq 3.2$		
9n	0.49	2.5	0.016	0.57	2.9	0.0064
275n	0.57	2.9	0.5	0.61	3.1	0.1
8250n	0.73	3.7	20.0	0.80	4.1	14.0
82500n	0.78	4.0	140.0	0.86	4.4	20.3
	$M_S^c \simeq 0.7$			$M_S^c \simeq 0.7$		
9n	0.16	0.8	0.082	0.16	0.8	0.094
275n	0.18	0.9	3.8	0.17	0.9	4.0
8250n	0.24	1.2	71.0	0.21	1.1	81.0
82500n	0.27	1.4	480.0	0.23	1.2	806.0

^aInitial Alfvén Mach Number.

^bEstimated M_s from the measured linewidths.

^cActual M_s from original MHD simulations.

Mach number. When applying radiative transfer post processing we vary the density scaling factor by increasing and decreasing it by a factor of 30 from the standard numerical density of 275cm^{-3} ($\text{cm}^{-3} = n$ henceforth), which represents a typical value for a giant molecular cloud. We also include a very high density case with $82500n$. Each line of sight (LoS) has a spectral emission of ^{13}CO , with resolution of 0.5km s^{-1} and is taken perpendicular to mean magnetic field¹. The cube size of our clouds is $5pc$; gas temperature is $10K$; CO Abundance $[^{13}\text{CO}/\text{H}] = 1.5 \times 10^{-6}$.

2.1. Analysis of the Synthetic Observations

Once we generate the synthetic ^{13}CO line profile maps we measure the dispersion of the velocity profile using a Gaussian fit. Using a gas temperature of $T = 10K$ we can calculate the sonic Mach number as:

$$M_s = \frac{\sigma_{CO}^{3D}}{c_s} = \frac{\sqrt{3}\sigma_{CO}^{1D}}{c_s} \quad (2)$$

Where σ_{CO}^{1D} is the velocity dispersion in one dimension and c_s is the sound speed:

$$c_s = \sqrt{\frac{K_b T}{\mu m_H}} \quad (3)$$

In addition to the ^{13}CO simulations, we create synthetic dust maps using the column density maps from our MHD simulations with line-of-sight taken perpendicular to the mean magnetic field. We scale our column density mean value of unity to $2 \times 10^{22}\text{cm}^{-2}$ and then take a simple scaling law (see Bohlin et al. 1978) from column density to extinction as:

$$N_H = 1.9 \times 10^{21}\text{cm}^{-2} \frac{A_v}{\text{mag}} \quad (4)$$

We then disregarded the column densities with $A_v < 7\text{mag}$, following the procedure of KT13. In the left panel Figure 1 we show an example plot of the ^{13}CO line profiles for same supersonic super-Alfvénic simulation with different density values,

¹ A parallel LoS to magnetic field were considered in 4 cases to include low and high sonic(Alfvénic) Mach number, see section 3.

hence different optical depths. The opacity broadening effect slightly widens the observed profile. In the right panel of Figure 1 we show an example of the synthetic dust PDFs (with A_v cut off of 7) of simulations with subsonic(supersonic) Mach number. An increase in sonic Mach number broadens the dust column density PDF distribution.

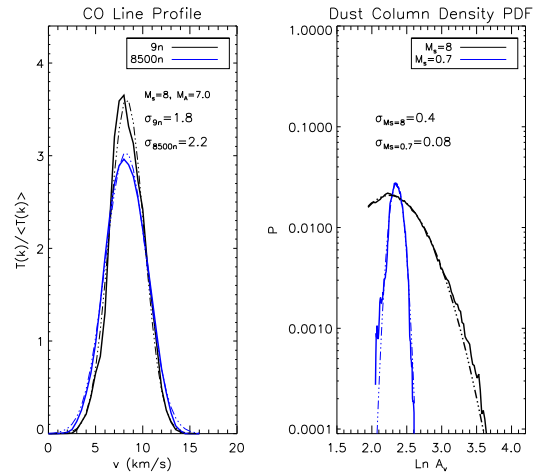


Fig. 1.— Left panel: ^{13}CO line profiles for same supersonic super-Alfvénic simulation with different density values. The solid line is the actual ^{13}CO line profile of densities $9n$ (black) and $8250n$ (blue) while thinner dashed line is a 3-term Gaussian fit using the native IDL routine GAUSSFIT. Right panel: Synthetic dust column density PDF for simulations with $M_s \approx 8$ (black) and $M_s \approx 0.7$ (blue); Thinner dashed lines is the corresponding Gaussian fit for the PDF.

In the following sections, we calculate the observed sonic Mach numbers from ^{13}CO line maps and compare this with the actual sonic Mach numbers as measured in the simulations. We also calculate the PDFs of the synthetic dust extinction maps and examine the standard deviation-sonic Mach number relationship as if it would have been calculated from the observations.

3. Sonic Mach Number from ^{13}CO Line Profiles

Figure 2 plots M_s as measured from the ^{13}CO line profiles (measured M_s) vs. actual M_s of the simulations. We plot four different values of density, which effectively change the optical depth (see Table 1). We also over plot linear fits to the sub-Alfvénic (blue lines) and super-Alfvénic (black lines) simulations separately with y-intercept held

to pass through the origin. We fit slopes to each optical depth regime and list the values in Table 2.

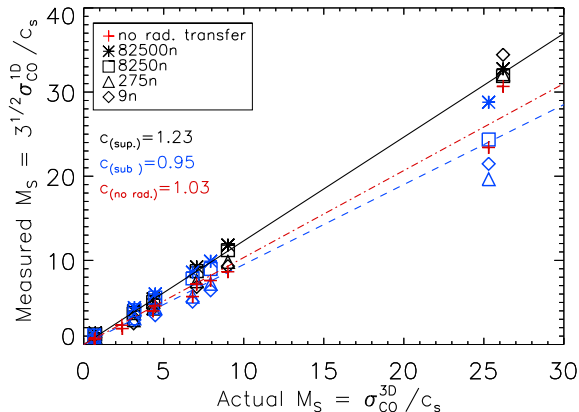


Fig. 2.— Measured M_s from ^{13}CO vs. actual M_s . Black solid line is a linear fit to the super-Alfvénic clouds; blue dashed line is for sub-Alfvénic clouds; red dot-dashed for no radiative transfer clouds.

We find that the optically thin cases (triangle and diamond symbols) reproduce well the actual sonic Mach number from the measured one. However, for our highest optical depth cases the ratio between the observationally measured M_s and the actual M_s increase to between $\approx 1.16 - 1.3$ (fitted slopes are reported in Table 2). An additional line broadening due to opacity enlarges the discrepancy between the measured and actual M_s as the optical depth increases. This occurs because the center of line emission becomes saturated and photons escape the cloud at the wings of the emission line. Indeed, CO opacity broadening can be explained from the curve-of-growth relationship as well as numerous past studies (Lepine 1991; Leung & Brown 1977; Leung & Liszt 1976, see Table 2).

Additionally, we observe a magnetic field dependency: super-Alfvénic turbulence shows increased line broadening as compared with sub-Alfvénic turbulence for all values of optical depth for supersonic turbulence. This effect maybe due to the velocity dispersion of super-Alfvénic turbulence having a larger dependency on density fluctuations for supersonic turbulence (see Burkhart et al. 2009, Figures 9,10), which causes an additional broadening. This occurs regard-

less of the optical depth of the line (see Table 2). We investigated the effect of opacity broadening on a line-of-sight parallel to the mean magnetic field and found similar results to those reported in Figure 2: the slopes of the measured vs. actual M_s covering the range of optical depth values were 1.06 for sub-Alfvénic simulations and 1.28 for super-Alfvénic simulations. This indicates that the anisotropy present in MHD turbulence is not responsible for the line broadening and instead the strength of the magnetic field is more important.

4. Standard Deviation-Sonic Mach Number Relation

We utilize both our synthetic dust maps and ^{13}CO line dispersion data to estimate the standard deviation-sonic Mach number relation as it would be calculated from the observations and compare this with data from KT13. We calculate the standard deviation using two different methods. One is direct calculation of the column density standard deviation (σ_{direct}) divided by the mean value as:

$$\sigma_{N/\langle N \rangle} = \sqrt{\frac{1}{n} \sum_{i=1}^n \left(\frac{N_i}{\langle N \rangle} - \left\langle \frac{N_i}{\langle N \rangle} \right\rangle \right)^2} \quad (5)$$

The other method assumes a log-normal distribution and calculates the variance (σ_{lnN}^2) and mean (μ) values of the logarithm of the extinction maps by fitting a Gaussian distribution, illustrated in Figure 1 right panel. This method does not assume that we apriori know the actual mean value of the extinction distribution, as is indeed the case of the observations, however the assumption of log normality is not always appropriate for all molecular clouds as gravity creates deviations from the log-normal distribution (see Collins et al. 2012). From the fit we are able to determine the parameters μ and σ_{lnN}^2 , which are then used to calculate the mean ($\langle N \rangle$) and standard deviation (σ_N) of the corresponding log-normal distribution as:

$$\langle N \rangle = e^{\mu + \sigma_{lnN}^2/2} \quad (6)$$

and

$$\sigma_N = [(e^{\sigma_{lnN}^2} - 1)e^{2\mu + \sigma_{lnN}^2}]^{1/2} \quad (7)$$

For both methods, we calculate the standard deviation for a extinction distribution with an A_v

cut off of ≈ 7 for compatibility with the method used in KT13 (hence we denote these as $\sigma_{\text{dir,cut}}$ and $\sigma_{\text{lnN,cut}}$). We also investigate the standard deviation calculations for the complete A_v distribution. This is not available from observations, however it is interesting to see how large of a difference in the standard deviation is observed between this idealized case and a more realistic distribution with a low A_v cut off.

We find that there is not a substantial difference between the values of the standard deviation calculated either with equation 5 or equations 6, 7. This is expected for our data since we are dealing with log-normal distributions in the case of pure isothermal MHD turbulence. The differences of σ_{lnN} and σ_{direct} extend up to values of 0.15. We additionally find that there is not a large difference between the standard deviation of the full column density distribution and the column density distribution which employs a cut off value of $A_v = 7$. The differences between σ_{lnN} and σ_{direct} with a cut off value of $A_v = 7$ extend up to values of 0.13. However, for a sub-set of real clouds, it may be difficult to discern if one is dealing with a true log-normal distribution or beginnings of a high density power-law tail thus the difference in using direct calculation *vs.* a log-normal fit for the calculation of the standard deviation of the column density in observational clouds might be higher.

Figure 3 shows the column density dispersion for the four different methods of calculating the standard deviation: σ_{direct} , $\sigma_{\text{dir,cut}}$, σ_{lnN} and $\sigma_{\text{lnN,cut}}$ (direct calculation, direct calculation with $A_v = 7$ cut off, log-normal fit, log-normal fit with $A_v = 7$ cut off, respectively) *vs.* estimated M_s for sub-Alfvénic (top panel) and super-Alfvénic cases (bottom panel). The values of M_s plotted are the average M_s calculated from the line widths of the four density cases with error bars representing the standard deviation between the values. We perform a linear fit to the [measured M_s , $\sigma_{N/\langle N \rangle}$] data, as used in KT13,

$$\sigma_{N/\langle N \rangle} = a_1 \times M_s + a_2 \quad (8)$$

Where a_1 is the slope between sonic Mach number and column density dispersion and a_2 is the intercept.

Along with the synthetic observations presented in this paper, Figure 3 overplots data from

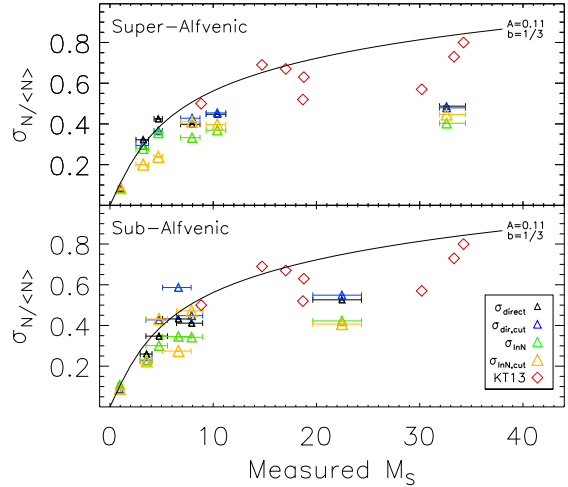


Fig. 3.— Column Density dispersion *vs.* measured M_s for super-Alfvénic (upper panel) and sub-Alfvénic (lower panel) cases. Clouds from KT13 table 1 as used in their Figure 7 left frame are shown as red losanges. Black line is a fit to theoretical prediction from BL12.

the IRDCs presented in KT13 (their Figure 7 left frame – M_s from a Gaussian fit, and reported in KT13 Table 1) which are shown with red diamond symbols. The KT13 values of $\sigma_{N/\langle N \rangle}$ plotted here are calculated by method of direct calculation, and thus most compatible with our method of direct calculation with $A_v=7$ cut off (blue triangles). Additionally, we include the predicted relation for the column density standard deviation - sonic Mach number relation from BL12, eq. 4 with $b = 1/3$ for solenoidal mixing and $A = 0.11$:

$$\sigma_{N/\langle N \rangle} = \sqrt{(b^2 M_s^2 + 1)^A - 1} \quad (9)$$

The observational points of KT13 consistently show higher values of σ than the MHD simulations, regardless of the method of calculation for the standard deviation or the Alfvén Mach number. Upon further inspection, the KT13 points also have a spread in the values of σ for a given sonic Mach number, suggesting that other physics might come into play in the interpretation of the variance of the data. Processes that could create larger values of variance than expected from solenoidally driven turbulence include gravitational contraction (Collins et al.

TABLE 2

SLOPE (DENOTED AS c) FOR THE MEASURED M_S -ACTUAL M_S DATA FIT. COLUMN TWO IS THE SLOPE FOR A FIT INCLUDING $M_S > 20$. COLUMN THREE IS FOR A FIT WITH $M_S < 20$.

	c^a	c^b
Super-Alfvénic		
$9n$	1.25	0.99
$275n$	1.19	1.06
$8250n$	1.22	1.23
$82500n$	1.26	1.30
Sub-Alfvénic		
$9n$	0.84	0.80
$275n$	0.80	0.90
$8250n$	1.00	1.17
$82500n$	1.16	1.28

^aIncluding $M_S > 20$.

^bOnly for $M_S < 20$

2012) and compressive forcing (Federrath et al. 2010; Kainulainen et al. 2013).

Comparing the mean value of the slopes for the cases of direct calculation of the standard deviation with the A_v cut off, $a_1 = 0.0103 \pm 0.0047$ (0.0136 ± 0.0050 for sub-Alfvénic; 0.0069 ± 0.0044 for super-Alfvénic), with KT13 Figure 7 left frame, which reports $a_1 = 0.0095 \pm 0.0066$, we see that there is a good agreement. We see significantly less agreement of our a_1 values from the values of standard deviation derived from the fitted log-normals, $a_1 = 0.0110 \pm 0.0067$ (0.0133 ± 0.0089 for sub-Alfvénic; 0.0086 ± 0.0046 for super-Alfvénic), with those of KT13 (their Fig. 8, left frame), $a_1 = 0.051 \pm 0.018$. The discrepancy maybe due PDF broadening by gravity in the observations (i.e. an unresolved power law tail), thus distorting the standard deviation’s relationship to the sonic Mach number.

The other possible explanation for a steeper relation could be that the driving in the KT13 data is compressive forcing, however they derived an expression for b ,

$$b = \frac{\sigma_{\rho}/\langle\rho\rangle}{M_s} = \frac{\sigma_{N/\langle N\rangle}}{M_s} R^{-1/2} = a_1 \times R^{-1/2} \quad (10)$$

where R is the 3D–2D variance ratio and was found to be between $R=[0.03, 0.15]$ (Brunt (2010)). KT13 estimated a b value with 3- σ uncertainty of $b = 0.20^{+0.37}_{-0.22}$, which indicates that the

driving is generally solenoidal to mixed ($b=1/3$ for solenoidal and $b=1$ for compressive driving, Federrath et al. 2008).

However, it is clear that applying a sonic Mach number opacity correction in the case of high optical depths will increase the measured value of b , since the slope a_1 will steepen by the correction factor. In the case of high optical depth this factor is as high as ≈ 1.3 . Thus the slope, a_1 , steepens by this factor and, assuming the observations are optically thick, the value of b calculated by KT13 will increase to $b = 0.25^{+0.25}_{-0.15}$. These values still indicate solenoidal to mixed driving. Hence the most likely explanation of higher variance values in the KT13 as compared with simulations is the influence of gravity. This is not unexpected, as Collins et al. (2012, Table 1) shows that the variance measured from the PDFs in 3D density increases as gravity acts on the cloud.

5. Discussion

The models of star formation must invoke stirring by turbulence, including collecting matter by compressible turbulent motions (see McKee & Ostriker 2007, and ref. therein) and the removal of magnetic flux from the collapsing region by the process of reconnection diffusion, which is much faster than the traditionally considered process of ambipolar diffusion (Lazarian et al. 2012). This motivates observational quantitative studies of tur-

bulence and this paper is a part of such studies.

This paper studies the effect of self-absorption on the observational measurement of the sonic Mach number as measured from ^{13}CO linewidths with a range of densities and optical depths. ^{13}CO line broadening and extinction PDFs employed in this paper to study the sonic Mach number are in no way the only methods available to researchers to study turbulence in molecular clouds. Sonic² Mach numbers can be also successfully obtained with kurtosis and skewness of the PDF distribution (Kowal et al. 2007; Burkhart et al. 2009, 2010). Power spectra of density and velocity can be obtained with Velocity Channel Analysis (VCA) and Velocity Coordinate Spectrum (VCS) techniques (Lazarian & Pogosyan 1999, 2004, 2006) which were successfully tested numerically (see Chepurnov et al. 2008) and applied to HI and CO datasets (see Padoan et al. 2009; Chepurnov et al. 2010; Lazarian 2009, for a review). In view of complexity of astrophysical turbulence, a simultaneous use of the combination of these techniques presents an unquestionable advantage.

Our empirical finding is that the evaluation of the Mach number from the linewidth is possible even for strongly self-absorbing species, but a correction factor should be applied for opacity broadening. For the range of absorption depths that we studied we found that this correction factor is at most 1.3. It also corresponds to the earlier one dimensional studies of spectral line broadening in the presence of absorption in e.g. Leung & Brown (1977) and Leung & Liszt (1976). An additional consideration is that IRDCs are cold ($T = 10-40\text{K}$) and are likely to be close to isothermal, but if instead of 10K the cloud had a different temperature there would be a factor of $1/\sqrt{T}$ change in M_s .

6. Conclusions

We create synthetic ^{13}CO emission maps, with varying optical depth, and dust column density maps from a set of 3D MHD simulations. We de-

²One can also determine Alfvénic Mach number M_A using different contours of isocorrelation obtained with velocity centroids (see Esquivel & Lazarian 2010, and ref. therein), Tsallis statistics (Lazarian et al. 2012; Tofflemire et al. 2011), bispectrum (Burkhart et al. 2010, 2013b).

rive a standard deviation - sonic Mach number relation, as it would be found from the observations, and compare this with recent results from real clouds discussed in KT13. We find:

- Calculations of M_s from line widths of ^{13}CO are robust for optically thin ^{13}CO but are overestimated by a factor of up to ~ 1.3 for optically thick clouds. This is due to the well known, but often overlooked, effect of opacity broadening.
- This over estimation of the sonic Mach number as derived from ^{13}CO line widths will cause the slope of the $\sigma_{N/\langle N \rangle}$ - M_s relation to become more shallow and this will result in lower values of the measured b parameter.
- The $\sigma_{N/\langle N \rangle}$ values of clouds reported in KT13 are larger than values found from ideal solenoidally driven simulations of turbulence. This could be due to the fact that in real molecular clouds there exists the influences of gravity, which will increase the measured column density standard deviation.

We thank the anonymous referee for helpful comments. This work is supported by continuous grants from INEspaço/FAPERJ/CNPq/MCT. C.C. acknowledges a graduate PDSE/CAPES grant Process $n^\circ 9392/13 - 0$. B.B. acknowledges support from the Wisconsin Space grant. A.L. acknowledges the Vilas Associate Award and the NSF Grant AST-1212096. A.L. and B.B. acknowledge the Center for Magnetic Self-Organization in Laboratory and Astrophysical Plasmas and the IIP/UFRN (Natal) for hospitality. V.O. and J.S. acknowledge support from the Deutsche Forschungsgemeinschaft (DFG) project $n^\circ 0s 177/2 - 1$. V.O., J.S. and J.K. were supported by the central funds of the DFG-priority program 1573 (ISM-SPP).

REFERENCES

- Armstrong, J. W., Rickett, B. J., & Spangler, S. R. 1995, *ApJ*, 443, 209
- Beresnyak, A., Yan, H., & Lazarian, A. 2011, *ApJ*, 728, 60
- Bohlin, R. C., Savage, B. D., & Drake, J. F. 1978, *ApJ*, 224, 132

- Brunt, C. M. 2010, *A&A*, 513, A67
- Burkhart, B., Falceta-Gonçalves, D., Kowal, G., & Lazarian, A. 2009, *ApJ*, 693, 250
- Burkhart, B., Stanimirović, S., Lazarian, A., & Kowal, G. 2010, *ApJ*, 708, 1204
- Burkhart, B., Lazarian, A., & Gaensler, B. M. 2012, *ApJ*, 749, 145
- Burkhart, B., & Lazarian, A. 2012, *ApJ*, 755, L19 (BL12)
- Burkhart, B., Lazarian, A., Ossenkopf, V., & Stutzki, J. 2013a, *ApJ*, 771, 123
- Burkhart, B., Ossenkopf, V., Lazarian, A., & Stutzki, J. 2013b, *ApJ*, 771, 122
- Chepurnov, A., Gordon, J., Lazarian, A., & Stanimirovic, S. 2008, *ApJ*, 688, 1021
- Chepurnov, A., Lazarian, A., Stanimirović, S., Heiles, C., & Peek, J. E. G. 2010, *ApJ*, 714, 1398
- Chepurnov, A., & Lazarian, A. 2010, *ApJ*, 710, 853
- Cho, J., & Lazarian, A. 2003, *MNRAS*, 345, 325
- Collins, D. C., Kritsuk, A. G., Padoan, P., et al. 2012, *ApJ*, 750, 13
- Esquivel, A., & Lazarian, A. 2010, *ApJ*, 710, 125
- Federrath, C., Klessen, R. S., & Schmidt, W. 2008, *ApJ*, 688, L79
- Federrath, C., Roman-Duval, J., Klessen, R. S., Schmidt, W., & Mac Low, M.-M. 2010, *A&A*, 512, A81
- Gaensler, B. M., Haverkorn, M., Burkhart, B., et al. 2011, *Nature*, 478, 214
- Goldsmith, P. F., Heyer, M., Narayanan, G., et al. 2008, *ApJ*, 680, 428
- Goodman, A. A., Rosolowsky, E. W., Borkin, M. A., et al. 2009, *Nature*, 457, 63
- Heyer, M. H., Brunt, C., Snell, R. L., et al. 1998, *ApJS*, 115, 241
- Hill, A. S., Benjamin, R. A., Kowal, G., et al. 2008, *ApJ*, 686, 363
- Kainulainen, J., Beuther, H., Banerjee, R., Federrath, C., & Henning, T. 2011, *A&A*, 530, A64
- Kainulainen, J., Federrath, C., & Henning, T. 2013, *A&A*, 553, L8
- Kainulainen, J., & Tan, J. C. 2013, *A&A*, 549, A53 (KT13)
- Klessen, R. S., Heitsch, F., & Mac Low, M.-M. 2000, *ApJ*, 535, 887
- Kowal, G., Lazarian, A., & Beresnyak, A. 2007, *ApJ*, 658, 423
- Kowal, G., & Lazarian, A. 2007, *ApJ*, 666, L69
- Kowal, G., Lazarian, A., Vishniac, E. T., & Otmianowska-Mazur, K. 2009, *ApJ*, 700, 63
- Kowal, G., Falceta-Gonçalves, D. A., & Lazarian, A., 2011a, *New Journal of Physics*, 13, 053001
- Lazarian, A., & Vishniac, E. T. 1999, *ApJ*, 517, 700
- Lazarian, A., & Pogosyan, D. 1999, *Bulletin of the American Astronomical Society*, 31, 1449
- Lazarian, A., & Pogosyan, D. 2004, *ApJ*, 616, 943
- Lazarian, A., & Pogosyan, D. 2006, *ApJ*, 652, 1348
- Lazarian, A. 2009, *Space Sci. Rev.*, 143, 357
- Lazarian, A., Esquivel, A., & Crutcher, R. 2012, *ApJ*, 757, 154
- Lepine, J. R. D. 1991, *Fragmentation of Molecular Clouds and Star Formation*, 147, 451
- Leung, C.-M., & Liszt, H. S. 1976, *ApJ*, 208, 732
- Leung, C. M., & Brown, R. L. 1977, *ApJ*, 214, L73
- Lombardi, M., & Alves, J. 2001, *A&A*, 377, 1023
- McKee, C. F., & Ostriker, E. C. 2007, *ARA&A*, 45, 565
- Molina, F. Z., Glover, S. C. O., Federrath, C., & Klessen, R. S. 2012, *MNRAS*, 423, 2680
- Ossenkopf, V. 2002, *A&A*, 391, 295
- Padoan, P., Jones, B. J. T., & Nordlund, A. P. 1997, *ApJ*, 474, 730
- Padoan, P., Juvela, M., Kritsuk, A., & Norman, M. L. 2009, *ApJ*, 707, L153
- Peek, J. E. G., Heiles, C., Peek, K. M. G., Meyer, D. M., & Lauroesch, J. T. 2011, *ApJ*, 735, 129
- Tofflemire, B. M., Burkhart, B., & Lazarian, A. 2011, *ApJ*, 736, 60
- Vazquez-Semadeni, E. 1994, *ApJ*, 423, 681
- Yan, H., & Lazarian, A. 2004, *ApJ*, 614, 757

This 2-column preprint was prepared with the AAS L^AT_EX macros v5.2.